Figure 1. (a) Chemical vapor deposition (CVD) synthesis of nitrogen-doped carbon nanotube cups (NCNCs) and their mechanical separationvia probe-tip sonication. (b) Transmission electron microscopy (TEM) image of as-synthesized NCNC bers. (c) High-resolution TEM image showing one segment from a stacked NCNCber, the white dashed lines in the gure depict the directions of the graphitic walls and the tube axis, the white arrow shows the existence of amorphous carbon. (d) TEM image of an individual NCNC after mechanical separation. (e) High-resolution TEM image of an individual NCNC.

groups remains elusive, pyridinic nitrogen and graphitic nitrogen were considered as two main types of nitrogen functionalities in NCNCs.[30] Moreover, the existence of amino groups was also suggested based on NCNC reactivity [28,29] and acid base titration experiments.[31] In this work, we synthesized NCNCs by chemical vapor deposition (CVD) method and separated them into individual cups by treating them with a probe-tip sonicator. A number of microscopic and spectroscopic techniques were employed to scrutinize the morphological and chemical characteristics of NCNCs. We have found that individual separated NCNCs largely maintained their cup shape and graphitic structure as in their stacked forms, whereas their nitrogen functionalities became more distinct after the sonication process. By employing the Kaiser test and derivatized NCNCs with gold nanoparticles (NPs), we were able to quantitatively determine both the concentration and distribution of amine functionalities on NCNCs. By utilizing localized amine groups on the basal plane of the cups, we further managed to cover the opening of the cups with NPs as "stoppers", which demonstrated a new pathway to implement these cup-shaped carbon nanomaterials as nanoscale containers and drug delivery carriers.

RESULTS AND DISCUSSION

NCNCs were synthesized using a chemical vapor deposition (CVD) method from a mixture of 92.2 wt % xylenes, 7.0 wt % acetonitrile, and 0.75 wt % ferrocene as precursors (Figure 1a). At 800 °C under H_2 and Ar atmosphere, the precursor was injected into the CVD reactor at a rate of 1 mL/h. After 90 min of the reaction, NCNC product was formed as a thick carpet of a black material weighing 4−5 mg and was then peeled off by a razor blade and dispersed in ethanol. Transmission electron microscopy (TEM) images of the as-synthesized material (Figure 1b) show that NCNCs have diameters ranging from 20 to 50 nm and lengths up to 5 μm. Unlike undoped multiwalled carbon nanotubes (MWNTs) with a continuous hollow interior, tubular NCNCs consist of many conical compartments resembling the shape of stacked cups. The nanotube cups were stacked in a head-to-tail fashion along the common direction of the tube axis. Compared to our previous CVD synthesis method which used ethanol/acetonitrile/ferrocene as the precursors,[28] we noticed that by changing ethanol to xylene as the carbon source and decreasing the content of ferrocene catalyst, the shape and the diameters of resultant NCNCs became more uniform

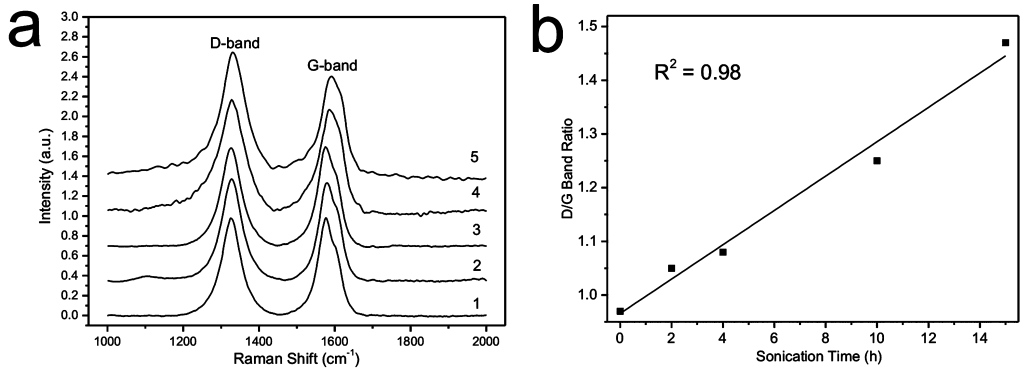

Figure 2. (a) Raman spectra of NCNCs after different duration of probe-tip sonication: (1) as-synthesized, (2) 2, (3) 4, (4) 10, and (5) 15 h. (b) Plot and linear fit of the D/G band ratio versus sonication time.

We assume that ethanol may introduce additional oxygen-containing defects in the graphitic structure[32] that may in turn affect the formation of the cup shape. The added ferrocene catalyst concentration is assumed to result in a more uniform size distribution of iron nanoparticles seeds. From TEM image (Figure 1b) it was occasionally observed that iron nanoparticles were encountered between the graphitic segments, delineating the innermost diameters of nanotubes.

High-resolution TEM images (Figure 1c) showed that the graphitic walls of stacked nanotubes were not parallel to the longitudinal axis, but were extended diagonally outward and terminated at the lateral surface. A layer of amorphous carbon was often observed at the surface with about 2 nm thickness. Owing to the size similarity, the cups were compactly nesting into each other's cavity taking up most the inner volume of the cup, with no interconnection of graphitic walls between each other. This observation indicated that the adjacent cups were not covalently connected but rather held together by the interlayer interaction. As a result, potential separation of individual nanotubes can be achieved via mechanical or chemical processes. Previous attempts of NCNC separation involving grinding with a mortar and pestle have obtained individual nanotubes out of their stacked structure only with a limited yield.[18] To improve the efficiency of separation, we applied probe-tip sonication to the sample after grinding. The sample was dispersed in DMF forming a stable suspension and then was treated with a 474 W probe sonicator for 5 h initially. The probe-tip sonication effectively broke the stacked compartments in the long range into short stacked cups and individual cups. The individual cups have common but moderately divided sweet shape and size, mostly ranging 50−200 nm in length and 30−50 nm in diameter (Supporting Information (S.I.) Figure S1). Figure 1d shows TEM image of a typical individual nanotube cup isolated from the stacking structure, having a semielliptical shape with the top sealed and the basal plane open. High-resolution TEM image (Figure 1e) revealed that the isolated individual nanotube cups maintained the graphitic structure on the sidewall where the parallel graphitic layers extended with a certain angle from the tube axis. The graphitic edge at the basal plane of the cup was distinctly depicted, which proved the three-dimensional cup shape morphology with open mouth to the hollow interior.

Although incompletely separated nanotube cups in short stacks of several units were frequently observed (S.I., Figure S1), the probe-tip sonication process significantly broke long NCNCs into smaller sections. On the basis of over 300 measurements obtained from TEM images, the average lengths of NCNCs showed a significant decrease with the sonication time (S.I., Figure S2). The length distribution histograms are revealed (Figure 2) decrease in the average length of NCNCs from ca. 43 μm to ca. 330 nm after 15 h of mechanical separation (S.I., Figure S2). A majority of over 70% NCNCs in the final sample ranged from 50 to 400 nm in length, corresponding to individual cups and short stacks of less than 10 units. Dynamic light scattering (DLS) measurements also showed that the length of NCNCs decrease from 2.2 ± 0.2 μm to 0.2 ± 5 nm after separation. While the DLS results may not reflect the actual length of nanotubes because the DLS measurement calculates the size based on hydrodynamic volume of the nanoparticles in solution, the result still reveals the significant trend of decreasing in the length of NCNCs as the result of probe-tip sonication.

Raman spectra further revealed that the probe-tip sonication process not only physically dissociated the nanotube cups from their stacks, but also cut more openings on the graphitic surface of nanotube cups. The relative intensity of D band (~1345 cm^{-1}) and G band (~1575 cm^{-1}) in Raman spectra are used to the extent of structural disorders of graphitic materials.[33] The Raman spectra were taken on samples after different durations of probe-tip sonication. Figure 2a shows the Raman spectra of NCNCs as-synthesized and after 2, 5, 10, and 15 h of sonication, normalized to the G band. The D to G band ratios were calculated and shown to increase linearly with the sonication time (Figure 2b). The increase in D/G band ratio was

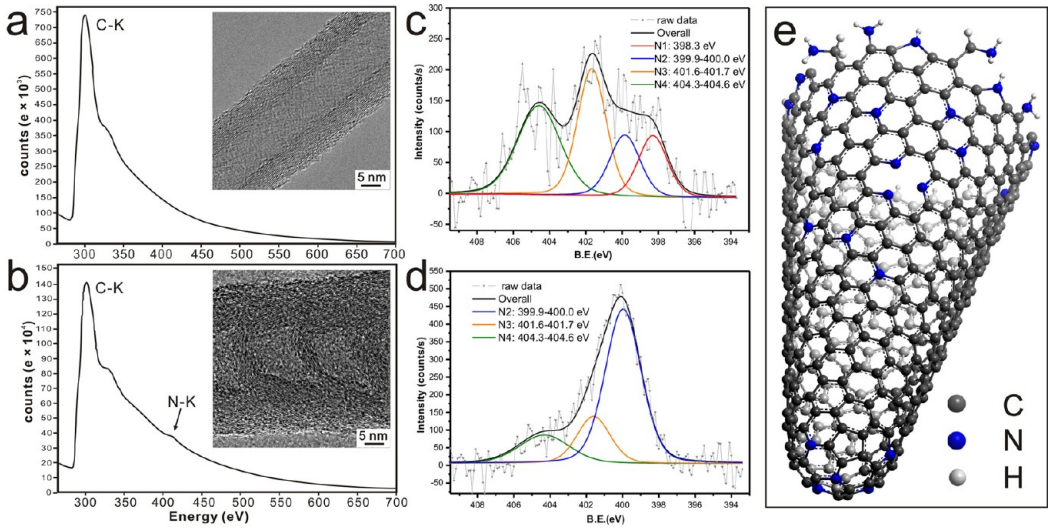

Figure 3. High-resolution TEM images (insets) and their corresponding electron energy loss spectroscopy (EELS) of (a) an uncompartmented section and (b) a compartmented section of NCNCs. X-ray photoelectron spectroscopy (XPS) of (c) as-synthesized NCNCs and (d) separated NCNCs after 15 h of sonication. (e) Structural scheme of one graphitic layer from separated NCNCs showing the varieties of possible nitrogen functionalities. This scheme is not drawn to scale.

acompanie with sigi ant ease in the eng th of NCNCs (S.I., Fig re S2) and ve ealed the e te of high-int esity ult ason ation on physical dissociation of et local nit ogen supply during the CVD p oces. On the ot he tion with tightly packed a bon a ticles (Fig re 1b the addition al signal a ising f om nit ogen K shell at 401 eV appea ed on the EELS spe t um, co esponding to a nit ogen conte t of about 1 2 at om% The e ist ibution of nit ogen conte t at the joint be t wee the adjacent cups was also visualized by EELS ele t on al mapping shown in S.I., Fig re S5, as the nit ogen signal show ed highe int esity at the inte-se tions of a short sta k of NCNCs. These esults suppo t the g owth mechanism of NCNCs in which nit ogen-doping lead s to the fo mation of cup-shaped o a bon a ticles st ucturing cu vatu es on the g aphitic ne tworks of the cups.

Ele t on al analysis ve ealed that the NCNCs have an ove all 1.0 at om% of nit ogen and 0.72 at om% of hydoge. X-ray photo ele t on spe t oscopy (XPS) fu the analyzed the nit ogen functionalities in both as-synthesized and sepa ated NCNC samples (Fig re 3c) shows nit ogen signals for both samples at about 400 eV. Since XPS only p obes the ele t on al composi-tion with in seve al nanome es f om the su face of the sample, it does not p obe nit ogen functionalities in bulk mate ials. Howeve, an inc ease in nit ogen con-ent ation was found f om 0.6 at om% in the as-synthesized NCNC sample to 0.5 at om% in the sepa ated sample, which may sugg st that more nit ogen functionalities we e exposed af e the p obe tip sonication p oces, possibly due to the emoval of su face amo phous a bon and the inc easing su-face a ea.

The ove all N1s p o le can be t ted into fou nit ogen compone ts. It is nece ary to ment ion that the sub anks for N1s high-esolution spe t a in

nitrogen-containing carbonaceous materials all have a relatively broad full width at half maximum (fwhm) around 2–3 eV due to the complicated chemical environment of nitrogen functionalities present at the heterogeneous carbon structure.[39] Therefore, the peaks were fitted by optimizing the peak shape and position at a Gaussian/Lorentzian ratio of 80:20 (S.I., Table S1).[40] Four peaks were involved to form the N1s profile of the as-synthesized NCNCs sample (Figure 3). The peak N1 at ~398.3 eV in the as-synthesized NCNCs may correspond to pyridinic nitrogen bonded with two carbon atoms in a six-membered ring structure.[41] The assignment of the peak N2 at 399.9–400.0 eV can be a bit difficult. While pyrrolic nitrogen is typically assigned at 400.1–400.6 eV,[41,42] this peak can be more likely associated to amine functionalities[39,43,44] The peak N3 at 401.6–401.7 eV may be assigned to graphitic (quaternary) nitrogen atoms which are tripled or bridged nitrogen incorporated in the graphitic networks by the substitution of carbon atoms.[39,45] The peak N4 at 404.3–404.6 eV may represent the molecular nitrogen which arises from the gaseous N_2 molecules interacted between the graphitic walls or trapped inside the cavities during the synthesis process.[46,47] After the pyridinic sonication, the separated NCNCs showed a bit different N1s profile (Figure 3). The peak N2 greatly increases with dominant intensity. We speculate that the increase of this peak results from the dissociation of nitrogen-containing compartments under the force of intense sonication. Presumably, the ablation to the outer graphitic layers not only causes removal of surface amorphous carbon and exposure of the existing amine functionalities, but also alters the local N frameworks and creates more dangling bonds such as amine. On the other hand, the peak N1 bare inidisting is absent in the separated NCNCs, which may partially due to the overshadowing of the shoulder of the peak N2, but may also indicate the transformation of pyridinic nitrogen to amine under sonication. After the separation process, there was a notable decrease in the peak N4, which may possibly due to the release of molecular N_2 once the cups were opened.

Fourier transform infrared spectroscopy (FT-IR) provided qualitative bonding information on the overall chemical functionalities of NCNCs (S.I., Figure S6). The spectra were taken on both as-synthesized and separated NCNCs dried in a vacuum oven. Because of their graphitic nature and limited functionalities, neither the samples showed strong IR intensities. However, in comparison to pristine MWNTs, the major absorption bands at ~3455 cm^{-1} may correspond to the N–H stretching vibration that arises from the potential pyrrolic or amine functionalities. Small increases were observed on the bands at 2850 and 2920 cm^{-1} after sonication, corresponding to the C–H vibrational

TABLE 1. **Primary Amine and Total Amine Loadings from Kaiser Test Results on As-Synthesized NCNCs and Separated NCNCs**[a]

	as-synthesized	separated
primary	not detected	1.06 ± 0.35 mol/g
total	0.85 ± 0.12 mol/g	2.76 ± 0.09 mol/g

[a] To obtain the total amine loadings, both samples were functionalized by Boc-Gly-OH and then deprotected off the Boc groups before the Kaiser test.

modes in methylene groups,[48] which support the assumption that the pyridinic sonication may damage the carbon sp^2 networks and create more saturated bonds. Two broad bands appearing at ~2920 and ~2850 cm^{-1} may be assigned to C–N and C=N stretching modes, respectively,[48] which may arise from pyridinic or graphitic QN functionalities. As a schematic illustration in Figure 3, the last two proposed morphology and structure of one graphitic layer of the separated NCNCs. Possible nitrogen functionalities such as pyridinic, graphitic nitrogen, and amine groups are shown based on the results of characterization.

Although the exact assignment of all nitrogen functionalities cannot be explicitly determined, the potential existence of amine functionalities is of particular interest because they can provide diverse reactivity for surface functionalization of NCNCs. Previously, the existence of amine groups on NCNCs was inferred based on the reactivity of NCNCs with (poly)ethylenimine in N-hydroxysuccinimide ester[8] and glutaraldehyde[2,49] In this work, type and amount of amine functionalities on NCNCs were first time quantitatively measured using a chemical colorimetric method known as the Kaiser test, which was widely applied for amine detection in peptide synthesis.[50] Both as-synthesized and separated samples were first analyzed without additional treatment. The test results showed the existence of primary amines on the separated NCNCs, but no primary amines were detected in the as-synthesized sample. The appearance of primary amines in separated NCNCs is consistent with the XPS results and supports our hypothesis that the pyridinic sonication can remove the surface amorphous carbon and create saturated structures such as primary amine. The primary amine loading in separated NCNCs was calculated as 1.06 ± 0.35 mol/g (Table 1), which was comparable to the literature value of amine loadings in NCNCs determined by an acid–base titration method.[31] It should be noted that the Kaiser test only detects the surface primary amines with hydrogen on the α-carbon, so presumably aromatic amines and other sp^2 nitrogen in NCNCs did not give a positive result (S.I., Figure S7). To quantify the total amine functionalities, NCNCs were functionalized with glycine molecules to yield primary amine terminals on the inherent amine groups. Both as-synthesized and separated NCNCs were reacted with Boc-protected glycine

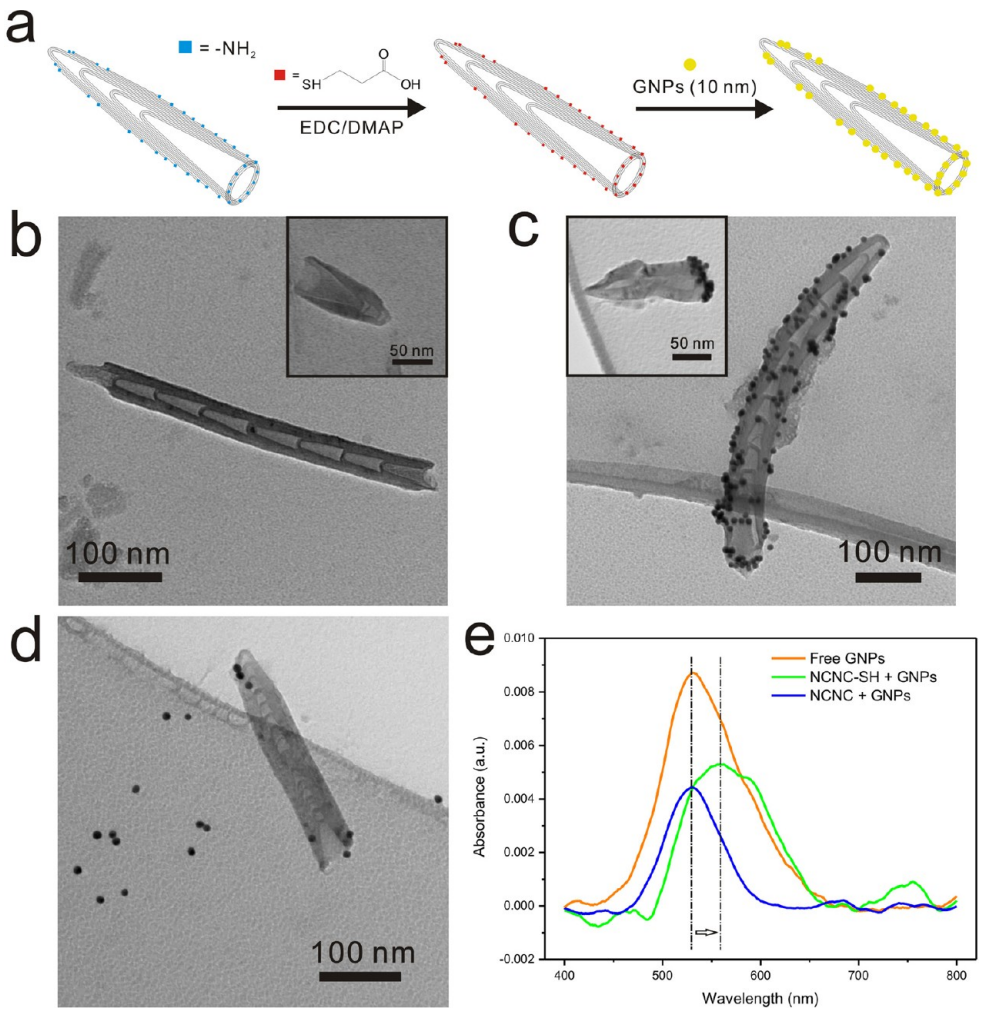

Figure 4. (a) Schematic illustration of functionalization of NCNCs with 10 nm gold nanoparticles (GNPs). (b,c) TEM images of separated NCNCs functionalized with 3-mercapto-propionic acid before (b) and after (c) attachment of GNPs. The insets in each panel show the corresponding images of individual NCNCs. (d) TEM image showing the distribution of GNPs among separated NCNCs without thiolation treatment. (e) UV vis spectra showing the surface plasmon resonance (SPR) band of GNPs with NCNC samples with or without thiolation treatment.

(N-(tert-butoxycarbonyl)-glycine, Boc-Gly-OH) through EDC coupling reaction, and the materials were repeatedly washed and photographed by the Boc groups to afford NCNC-glycine conjugates, on which the Kaiser test was performed. After glycine functionalization, the Kaiser test gave positive results on both as-synthesized and separated NCNC samples, indicating the inherent existence of aromatic amine on their surface. The total amine loading in separated NCNCs further increased almost twice after glycine functionalization (Table S1), showing that aromatic amine accounts for a large part of the total amine functionalities.

To confirm that the positive results were indeed attributed to amine functionalities, the amine-reactive sites on separated NCNCs were reacted with di-tert-butyl dicarbonate (Boc$_2$O) as illustrated in Scheme S1 to yield N-tert-butoxycarbonyl (NH-Boc) groups which protected the amine groups from the Kaiser test reactions. It turned out that Boc-protected NCNCs gave a negative Kaiser test result. Upon removal of Boc groups, amine groups were detected again (S.I., Scheme S1). The amine loading was 0.97 ± 0.07 mol/g which was close to that of separated NCNCs before any treatment, showing that that the protected amine groups could be almost completely revealed.

The existence of amine groups enabled facile surface functionalization of separated NCNCs. By EDC coupling reaction, we were able to add thiol functionalities, which have strong affinity to gold nanoparticles (GNPs) through Au–S interaction[9], to the amine terminals using 3-mercapto propionic acid (MPA, Figure 4a). The resulting thiolated nanocrystals showed no morphological identity from the unmodified ones. Figure 4b,c were separately washing and centrifugation, NCNCs were combined with citrate-stabilized GNPs with 10 nm diameters. From TEM images it was observed that GNPs were densely anchored on the surface of NCNCs (Figure 4c). On short stalked NCNCs, GNPs preferred to adsorb at the lower part of each section, especially at the bottom open rim. Because GNPs are

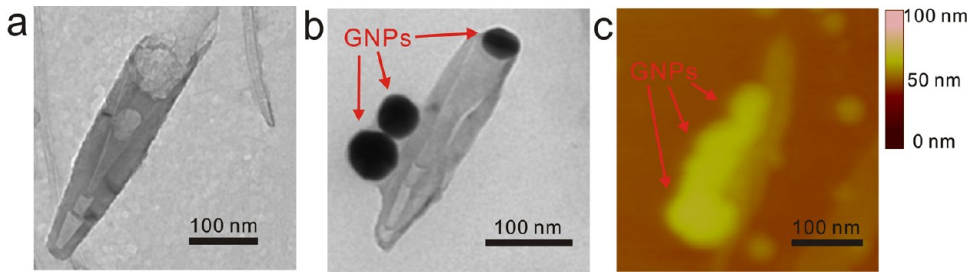

Figure 5. (a) TEM image of a NCNC retaining amorphous carbon inside the open cavity and (b) a thiolated NCNC corked with a 40 nm GNP and two other GNPs attached to its sidewall. (c) AFM contact-mode image of an individual NCNC functionalized with 40 nm GNPs.

bound to the thiolated amine sites, the distribution of GNPs and relatively provided "mapping" of amine functionalities on the surface of separated NCNCs. Theoretical calculations showed that the nitrogen-doping sites are more energetically favored to bind the subsequent growth of the graphitic network.[52] As amine groups are incompatible to the sp[2] networks, they are likely to stay at the edge of graphitic walls which eventually terminate at the surface of NCNCs. The inset in Figure 4c shows an individual NCNC functionalized with GNPs. The GNPs were preferentially attached on the open rim of the cup, marking the enrichment of amine functionalities at the opening. The interaction between GNPs and thiolated NCNCs is strong and specific. By simply mixing the GNPs with noncorked NCNCs in ethanol, few GNPs were randomly distributed throughout the sample with no specific interaction with NCNCs (Figure 4b). The GNPs can be easily washed off from noncorked NCNCs by centrifugation, but were bound strongly to thiolated NCNCs even after repeated washing. UV visible spectroscopy shows that the surface plasmon resonance (SPR) band for GNPs bound to thiolated NCNCs had a substantial redshift compared to free GNPs (Figure 4e), which may be caused by the specific interaction between GNPs and the thiol backbone ligands,[53] as well as the close proximity between adjacent GNPs.[54]

With their cup-shaped structure and localized amine reactive sites, separated NCNCs can be considered as nanoscale containers to accommodate various guest molecules inside their cavities. From TEM images of separated NCNCs, we frequently noticed some residual amorphous material retained in the open cavities of separated NCNCs. As shown in Figure 5a, in the short stalk of three cups, the open cup on top showed a darker color than the sealed cups at the bottom. This material was assumed to be amorphous carbon residues formed during the sonication process that were anchored on the inner graphitic walls of the cups due to their hydrophobic interaction (S.I., Figure S8). In addition, the preferential distribution of thiolated amine groups on the open edge allowed us to effectively "work" the opening of the cups using GNPs with appropriate size that fit the diameters of the cups. Figure 5b shows that when incubating thiolated NCNCs with 40 nm GNPs, one GNP can fit on the open rim of the cup and on the inner residual material inside. Individual thiolated NCNCs corked by GNP "stoppers" were frequently observed in the sample (S.I., Figure S9a). This working interaction between GNPs and NCNCs was fairly effective as plotted at a low magnification in Figure S9e, where the GNPs had preferentially worked on individual or short-stacked NCNCs at their open side. It was noted that the interactions were not exclusive on the open rims because GNPs may also bind to the thiol groups on the sidewalls of the cups due to their high aspect ratio (Figures 5b and 5c). GNPs attached on the open side might not necessarily have perfectly "working" (S.I., Figure S10). However, the "working" position is supposed to be thermodynamically more stable for 40 nm GNPs due to the entropy of thiol groups at the open rims and their fitting shapes. Statistically, there were 54% of short NCNCs functionalized with 40 nm GNPs, in which about 42% were worked, accounting for a percentage of ca. 23% worked NCNCs in total (S.I.). On average, each functionalized NCNC had about 2 GNPs, with over $^1/_3$ of them staying at the open side. Considering the high aspect ratio of NCNCs, the surface area of the sidewalls is roughly 9 times as that of the opening (S.I.), so the binding of GNPs to the open rims of NCNCs must be energetically favored. The atomic force microscopy (AFM) imaging in contact mode (Figure 5c) also confirmed the observation that GNPs with diameters about 40 nm tended to bind to the end of the individual NCNCs as well as on the sidewalls.

The preferential interactions between GNPs and thiolated amine groups on the open rims of the separated NCNCs were further confirmed using ESI elemental mapping in an energy filtered TEM (EFTEM) mode. Figure 6a shows a typical TEM image of a GNP bound to the opening of the thiolated NCNC. The GNP with 40 nm in diameter was slightly wider than the inner diameter of NCNCs and effectively worked at the cup. We recorded the corresponding elemental maps for Au, N, and S. The energy filtered image of Au O edge at 54 eV showed a bright sphere at the end of NCNC, confirming the chemical composition of GNPs (Figure 6a, inset). Nitrogen mapping taken at the N K edge of 401 eV revealed that nitrogen was mainly

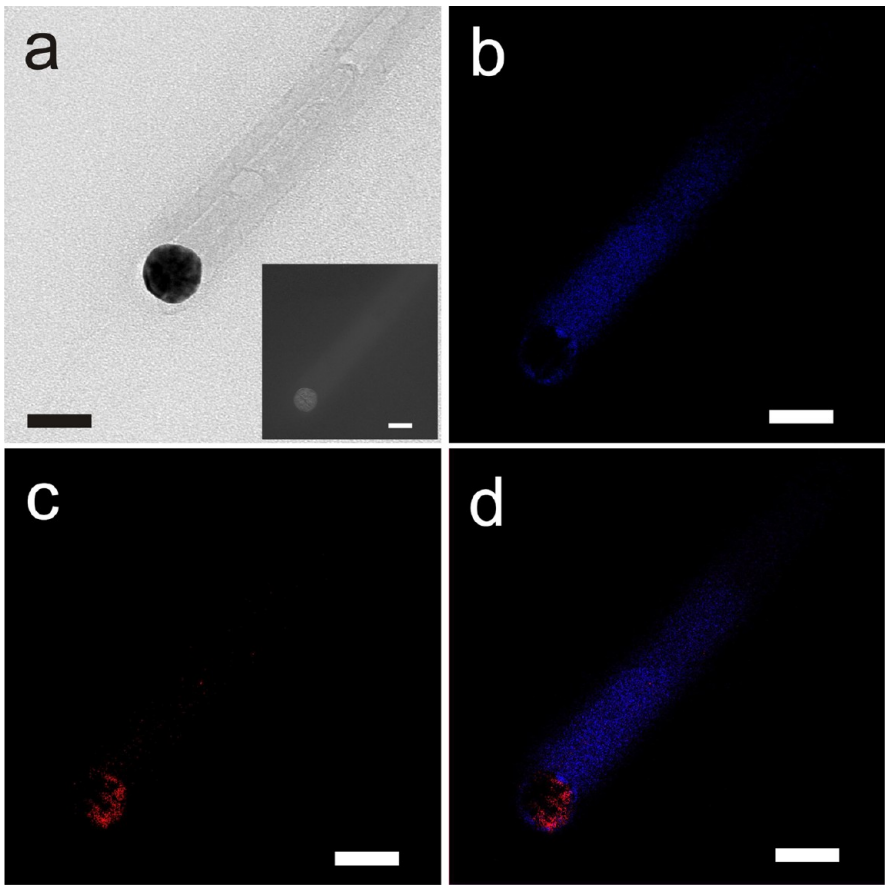

Figure 6. (a) TEM image of one GNP with 40 nm of diameter corking the opening of separated NCNCs. Inset: the energy filtered TEM (EFTEM) image of gold elemental mapping. (b,c) EFTEM images for nitrogen (colored blue) and sulfur (colored red) and (d) overlap of images b and c. All scale bars represent 40 nm.

distributed at the lower part of NCNC (Figure 6b). Notably, the elemental mapping for sulfur at the S L edge (165 eV) showed the enrichment of thiol groups at the open end of the NCNC, which essentially reveal the localized distribution of amine functionalities (Figure 6c,d). The thiol groups shared the same position as GNPs, which actually proved the mechanism of the "working" behavior between GNPs and thiolated NCNCs.

Because of the chemical nature of the localized amine functionalities, the working materials were not exclusive to GNPs. Silver nanoparticles can also have strong affinity to thiols and were able to stop the NCNCs as well (S.I., Figure S1). Furthermore, by introducing 40 nm polystyrene latex nanoparticles containing alkylene groups to separated NCNCs in ethanol, NCNCs can also trap the polymer nanoparticles with no need of further functionalization, presumably due to the formation of imine bonds (S.I., Figure S2). The similar working behavior was also observed in another study using amine functionalized silica nanotest tubes.[55] Our experimental results point to the application of NCNCs as graphitic nanoscale containers which can be worked with hidden heat nanoparticles. These hybrid carbon nanocomposite or polymer nanoparticle nanoassemblies can be explored as multifunctional vehicles for applications such as drug delivery and biological targeting. Future in vivo studies on these nanomaterials are necessary to test their effectiveness for the biological applications.

CONCLUSION

We introduced a new methodology to obtain individual NCNCs using probe ipsonication. We showed that this method can effectively separate NCNCs from their stacked structure. TEM images revealed that separated NCNCs largely exist as individuals or short stacks with less than 400 nm in length, and maintained their cup-shaped structures with more graphitized. Spectroscopic characterization showed the existence of different nitrogen functionalities in separated NCNCs that are responsible for their cup-shaped morphology. By adopting the Kaiser test, we quantified the type and concentration of amine functionalities on the surface of NCNCs, which are particularly interesting due to their diverse reactivity. By thiolation of the amine groups and functionalization with GNPs, we were able to visualize the distribution of amine groups on NCNCs and found that they were preferentially located at the open basal plane of the cups.

Taking advantage of these groups, we managed to derivatize these NCNCs with large NMR signals as "markers" or "stoppers" due to the localized aminediol distribution, which was proved by TEM elemental mapping. These novel nanohybrid nanomaterials showed versatile properties toward molecular recognition and manipulation, and may lead to potential applications such as nanoscale containers and drug delivery systems.

MATERIALS AND METHODS

Catalyst materials: gold nanoparticles with 10 nm diameters and silver nanoparticles with 40 nm diameters were purchased from Sigma Aldrich, and citrate-coated gold nanoparticles with 40 nm diameters were purchased from nanoComposix. Alkyne-functionalized latex nanoparticles were purchased from invitrogen. MWNTs (Bayt ubes) were received from Bayer Material Science as a generous gift. All other analytical grade reagents and solvents were purchased from Sigma Aldrich and used as received.

Growth of NCNCs *via* Chemical Vapor Deposition (CVD). NCNCs were synthesized using CVD technique in a Lindberg/Blue tube furnace. NCNCs were grown on a quartz substrate placed in a quartz tube (1 in. diameter) inside the furnace. A liquid precursor containing 7.0 wt % of acetonitrile, 0.75 wt % of ferrocene, and 92.2 wt % of xylene was injected at a rate of 1 mL/min under a H_2 (97.5 sccm) and Ar (48 sccm) atmosphere. The system was maintained at 800 °C for 90 min and then allowed to cool down under an Ar atmosphere for 1 h. NCNC product formed a black coating on the quartz substrate wall and was then scraped off and collected using a razor blade.

Mechanical Separation of As-Synthesized NCNCs into Individual Cups. Approximately 5 mg of as-synthesized NCNCs (as-grown first) were transferred to an agate mortar and pestle to which several drops of EtOH were added. After 30 min of grinding, the sample was collected and dispersed in 2 mL of DMF. The suspension was then processed under Sonics & Materials VCX-600 ultrasonicator (as-obtained equipped with a $\frac{1}{4}$ in. titanium microprobe at 60% of its maximal amplitude for 0.5 h in an ice bath. The resultant NCNC suspensions were then centrifuged to remove any large particles.

Decoration of NCNCs with Gold Nanoparticles. The separated NCNCs were first thiolated by reaction with 3-mercaptopropionic acid (MPA) through EDC coupling reaction. Approximately 0.1 mg of separated NCNCs were suspended in 4 mL of DMF. To the suspension, 2 mL of MPA (2 mg of ethyl-3-(3-dimethylaminopropyl) carbodiimide (EDC) and 4 mg of 4-dimethylaminopyridine (DMAP) were added and the mixture was stirred under N_2 at room temperature overnight. After rinsed with EtOH, the thiolated NCNC suspension in EtOH was incubated overnight with citrate-coated GNPs with diameters of either 10 or 40 nm.

Conflict of Interest: The authors declare no competing financial interest.

Acknowledgment. Dedicated to Professor Sir J. Fraser Stoddart on the occasion of his 70th birthday. This work was supported by an NSF (CBET Award No. 0953845). The authors thank NFFE at the University of Pittsburgh and especially D. Sushengtan for the provision of assistance to the instrumentation and assistance. We gratefully acknowledge R. J. Lee group for access to the XPS instrumentation and Professor R. A. Buttera for his comments on the XPS data analysis.

Supporting Information Available: Supplemental experimental procedure and calculations; TEM images of separated NCNCs; length distribution of as-synthesized and separated NCNCs; high-resolution TEM images of armchair graphitic lattice; Raman spectra of NCNCs with different defect loadings; ET-TEM elemental mapping of separated NCNCs; FT-IR spectra of undoped MWNTs, as-synthesized and separated NCNCs; Kaiser test results of 8-aminoquinoline and glycine; high-resolution TEM images of amorphous carbon residue in NCNCs; TEM images of NCNCs cork with GNPs; TEM images of GNPs attached on NCNCs without the confirmations; TEM images of NCNCs cork with silver and polystyrene latex nanoparticles; schematic of Boc_2O protection and deprotection of NCNCs; table of fitting peak information of XPS spectra. This material is available free of charge via the Internet at http://pubs.acs.org.

REFERENCES AND NOTES

1. Baughman, R. H.; Zakhidov, A. A.; de Heer, W. A. Carbon Nanotubes—The Route toward Applications. *Science* **2002**, *297*, 787–792.
2. Odom, T. W.; Huang, J.-L.; Kim, P.; Lieber, C. M. Structure and Electronic Properties of Carbon Nanotubes. *J. Phys. Chem. B* **2000**, *104*, 2794–2809.
3. Tasis, D.; Tagmatarchis, N.; Bianco, A.; Prato, M. Chemistry of Carbon Nanotubes. *Chem. Rev.* **2006**, *106*, 1105–1136.
4. Sgobba, V.; Guldi, D. M. Carbon Nanotubes—Electronic/Electrochemical Properties and Application for Nanoelectronics and Photonics. *Chem. Soc. Rev.* **2009**, *38*, 165–184.
5. Gao, J.; Gao, S.; Zhao, X.; Kuznetsova, L. V.; Wong, S. S.; Ojima, I. Functionalized Single-Walled Carbon Nanotubes as Rationally Designed Vehicles for Tumor-Targeted Drug Delivery. *J. Am. Chem. Soc.* **2008**, *130*, 6778–6785.
6. Kam, N. W. S.; Liu, Z.; Dai, H. Functionalization of Carbon Nanotubes via Cleavable Disulfide Bonds for Efficient Intracellular Delivery of siRNA and Potent Gene Silencing. *J. Am. Chem. Soc.* **2005**, *127*, 12492–12493.
7. Cruz-Silva, E.; Cullen, D. A.; Gu, L.; Romo-Herrera, J. M.; Muñoz-Sandoval, E.; López-Urías, F.; Sumpter, B. G.; Meunier, V.; Charlier, J.-C.; Smith, D. J.; *et al.* Heterodoped Nanotubes: Theory, Synthesis, and Characterization of Phosphorus-Nitrogen-Doped Multiwalled Carbon Nanotubes. *ACS Nano* **2008**, *2*, 441–448.
8. Yang, L.; Jiang, S.; Zhao, Y.; Zhu, L.; Chen, S.; Wang, X.; Wu, Q.; Ma, J.; Ma, Y.; Hu, Z. Boron-Doped Carbon Nanotubes as Metal-Free Electrocatalysts for the Oxygen Reduction Reaction. *Angew. Chem., Int. Ed.* **2011**, *50*, 7132–7135.
9. Blake, R.; Gunko, Y. K.; Coleman, J.; Cadek, M.; Fonseca, A.; Nagy, J. B.; Blau, W. J. A Generic Organometallic Approach toward Ultrastrong Carbon Nanotube-Polymer Composites. *J. Am. Chem. Soc.* **2004**, *126*, 10089–10092.
10. Kauffman, D. R.; Star, A. Carbon Nanotube Gas and Vapor Sensors. *Angew. Chem., Int. Ed.* **2008**, *47*, 6550–6570.
11. Allen, B. L.; Kichambare, P. D.; Star, A. Carbon Nanotube Field-Effect-Transistor-Based Biosensors. *Adv. Mater.* **2007**, *19*, 1439–1451.
12. Liu, Z.; Chen, K.; Davis, C.; Sherlock, S.; Cao, Q.; Chen, X.; Dai, H. Drug Delivery with Carbon Nanotubes for in Vivo Cancer Treatment. *Cancer Res.* **2008**, *68*, 6652–6660.
13. Wu, W.; Wieckowski, S.; Pastorin, G.; Benincasa, M.; Klumpp, C.; Briand, J.-P.; Gennaro, R.; Prato, M.; Bianco, A. Targeted Delivery of Amphotericin B to Cells by Using Functionalized Carbon Nanotubes. *Angew. Chem., Int. Ed.* **2005**, *44*, 6358–6362.
14. Wang, E. G. Nitrogen-Doped Carbon Nanotubes and Their Properties. *J. Mater. Res.* **2006**, *21*, 2767–2773.
15. Terrones, M.; Ajayan, P. M.; Banhart, F.; Blase, X.; Carroll, D. L.; Charlier, J.-C.; Czerw, R.; Foley, B.; Grobert, N.; Kamalakaran, R.; *et al.* N-Doping and Coalescence of Carbon Nanotubes: Synthesis and Electronic Properties. *Appl. Phys. A* **2002**, *74*, 355–361.
16. Maldonado, S.; Morin, S.; Stevenson, K. J. Structure, Composition, and Chemical Reactivity of Carbon Nanotubes by Selective Nitrogen Doping. *Carbon* **2006**, *44*, 1429–1437.
17. Bai, X. D.; Zhong, D.; Zhang, G. Y.; Ma, X. C.; Liu, S.; Wang, E. G.; Chen, Y.; Shaw, D. T. Hydrogen Storage in Carbon Nitride Nanotubes. *Appl. Phys. Lett.* **2001**, *79*, 1552–1554.

18. Zhong, D.Y.; Zhang, G.Y.; Liu, S.; Wang, E.G.; Wang, Q.; Li, H.; Huang, X. J. Lithium Storage in Polymerized Carbon Nitride Nanotubes. *Appl. Phys. Lett.* **2001**, *79*, 3500–3502.
19. Gong, K.; Du, F.; Xia, Z.; Durstock, M.; Dai, L. Nitrogen-Doped Carbon Nanotube Arrays with High Electrocatalytic Activity for Oxygen Reduction. *Science* **2009**, *323*, 760–764.
20. Tang, Y.; Allen, B.L.; Kauffman, D.R.; Star, A. Electrocatalytic Activity of Nitrogen-Doped Carbon Nanotubes. *J. Am. Chem. Soc.* **2009**, *131*, 13200–13201.
21. Carrero-Sánchez, J.C.; Elías, A.L.; Mancilla, R.; Arellín, G.; Terrones, H.; Laclette, J.P.; Terrones, M. Biocompatibility and Toxicological Studies of Carbon Nanotubes Doped with Nitrogen. *Nano Lett.* **2006**, *6*, 1609–1616.
22. Zhao, M.L.; Li, D.J.; Yuan, L.; Yue, Y.C.; Liu, H.; Sun, X. Decrease in Cytocompatibility and Hemocompatibility between Carbon Nanotubes and Nitrogen-Doped Carbon Nanotubes. *Carbon* **2011**, *49*, 3181–3188.
23. Zhao, Y.; Allen, B.L.; Star, A. Enzymatic Degradation of Multiwalled Carbon Nanotubes. *J. Phys. Chem. A* **2011**, *115*, 9536–9544.
24. Kornev, K.; Ye, H.; Grigoriev, Y.; Grotsi, Y.; Halverson, D.; Friedman, G.; Bradley, J.C.; Kornev, K.G. Carbon Nanotubes Loaded with Magnetic Particles. *Nano Lett.* **2005**, *5*, 879–884.
25. Kim, B.M.; Qian, S.; Bau, H.H. Filling Carbon Nanotubes with Particles. *Nano Lett.* **2005**, *5*, 873–878.
26. Sethil Kumar, A.; Swetha, P. Electrochemical Assisted Encapsulation of Cytochrome on a Multiwalled Carbon Nanotube Modified Electrode. *Langmuir* **2010**, *26*, 6874–6877.
27. Shekunov, B.; Chattopadhyay, P.; Tong, H.; Chow, A. Particle Size Analysis in Pharmaceutics: Principles, Methods and Applications. *Pharm. Res.* **2007**, *24*, 203–227.
28. Allen, B.L.; Kichambare, P.D.; Star, A. Synthesis, Characterization, and Manipulation of Nitrogen-Doped Carbon Nanotubes. *ACS Nano* **2008**, *2*, 914–920.
29. Allen, B.L.; Shaver, C.M.; Yingling, A.M.; Perouel, S.; Star, A. Graphitic Nanocapsules. *Adv. Mater.* **2009**, *21*, 4692–4695.
30. Terrones, M.; Jorio, A.; Endo, M.; Rao, A.M.; Kim, Y.A.; Hayashi, T.; Terrones, H.; Charlier, J.C.; Dresselhaus, G.; Dresselhaus, M.S. New Direction in Nanotube Science. *Mater. Today* **2004**, *7*, 30–45.
31. Bittel, J.H.; van Dommelen, S.; Long, K.P. On the Virtue of Acid Base Titrations for the Determination of Basic Sites in Nitrogen-Doped Carbon Nanotubes. *Catal. Today* **2010**, *150*, 61–66.
32. Castle, A.B.; Garcia-Pomar, E.; Nieto-Delgado, C.; Terrones, H.; Terrones, M.; Hussain, S. Hydroxyl-Functionalized and N-Doped Multiwalled Carbon Nanotubes Decorated with Silver Nanoparticles Preserve Endothelial Function. *ACS Nano* **2011**, *5*, 2458–2466.
33. Dresselhaus, M.S.; Jorio, A.; Hofmann, M.; Dresselhaus, G.; Saito, R. Perspectives on Carbon Nanotubes and Graphene Raman Spectroscopy. *Nano Lett.* **2010**, *10*, 751–758.
34. Cançado, L.G.; Jorio, A.; Ferreira, E.H.M.; Stavale, F.; Achete, C.A.; Capaz, R.B.; Moutinho, M.V.O.; Lombard, A.; Kulmala, T.S.; Ferrari, A.C. Quantifying Defects in Graphene via Raman Spectroscopy at Different Excitation Energies. *Nano Lett.* **2011**, *11*, 3190–3196.
35. Zhang, G.Y.; Ma, X.C.; Zhong, D.Y.; Wang, E.G. Polymerized Carbon Nitride Nanotubes. *J. Appl. Phys.* **2002**, *91*, 9324–9332.
36. Mandrimal, J.; Gröning, S.; Seefeldt, G. Curvature Effects of Nitrogen on Graphitic Sheets: Structure and Energetics. *Chem. Phys. Lett.* **2007**, *447*, 51–54.
37. Lin, M.; Tan, J.P.Y.; Boothroyd, C.; Loh, K.P.; Tok, E.S.; Foo, Y.L. Dynamical Observation of Bamboo-like Carbon Nanotube Growth. *Nano Lett.* **2007**, *7*, 2234–2238.
38. Wang, Y.; Bai, X. High-Yield Preparation of Individual Nitrogen-Containing Carbon Nanotubes. *Mater. Lett.* **2009**, *63*, 2606–2608.
39. Pels, J.R.; Kapteijn, F.; Moulijn, J.A.; Zhu, Q.; Thomas, K.M. Evolution of Nitrogen Functionality in Carbonaceous Materials During Pyrolysis. *Carbon* **1995**, *33*, 1641–1653.
40. Wagner, C.D. *Handbook of Monochromatic XPS Spectra: The Elements and Native Oxides*; Wiley: Hoboken, NJ, 2000; p 29–82.
41. Kundu, S.; Nagaiah, T.C.; Xia, W.; Wang, Y.; Dommele, S. V.; Bitter, J.H.; Santa, M.; Grundmeier, G.; Bron, M.; Schuhmann, W.; et al. Electrocatalytic Activity and Stability of Nitrogen-Containing Carbon Nanotubes in the Oxygen Reduction Reaction. *J. Phys. Chem. C* **2009**, *113*, 14302–14310.
42. Casanovas, J.; Ricart, J.M.; Rubio, J.; Illas, F.; Jiménez-Mateos, J.M. Origin of the Large N 1s Binding Energy in X-ray Photoelectron Spectra of Calicene and Carbon Nanotube Materials. *J. Am. Chem. Soc.* **1996**, *118*, 8071–8076.
43. Ramanathan, T.; Fisher, F.T.; Ruoff, R.S.; Brinson, L.C. Amino-Functionalized Carbon Nanotubes for Binding to Polymers and Biological Systems. *Chem. Mater.* **2005**, *17*, 290–298.
44. Jansen, R.J.J.; van Bekkum, H. XPS of Nitrogen-Containing Functional Groups on Activated Carbon. *Carbon* **1995**, *33*, 1021–1027.
45. van Dommele, S.; Romero-Izquirdo, A.; Brydson, R.; de Jong, K.P.; Bitter, J.H. Tuning Nitrogen Functionality in Catalytically Grown Nitrogen-Containing Carbon Nanotubes. *Carbon* **2008**, *46*, 138–148.
46. Liu, H.; Zhang, Y.; Li, R.; Sun, X.; Désilets, S.; Abou-Rachid, H.; Jaidann, M.; Lussier, L.S. Structural and Morphological Control of Aligned Nitrogen-Doped Carbon Nanotubes. *Carbon* **2010**, *48*, 1498–1507.
47. Zhou, J.; Wang, J.; Liu, H.; Banis, M.N.; Sun, X.; Sham, T.K. Imaging Nitrogen in Individual Carbon Nanotubes. *J. Phys. Chem. Lett.* **2010**, *1*, 709–713.
48. Guan, L.H.; Hong, K.H.; Xiao, D.Q.; Lin, T.C.; Lai, S.H.; Hsieh, W.J.; Shih, H.C. Resolution of the Binding Configuration in Nitrogen-Doped Carbon Nanotube. *Phys. Rev.* **2004**, *70*, 2408.
49. Allen, B.L.; Kichambare, M.D.; Star, A. Controlling the Volumetric Parameters of Nitrogen-Doped Carbon Nanotube Cups. *Nanoscale* **2010**, *2*, 1605–1608.
50. Sarin, V.K.; Kent, S.B.; Tam, J.P.; Merrifield, R.B. Quantitative Monitoring of Solid-Phase Peptide Synthesis by the Ninhydrin Reaction. *Anal. Biochem.* **1981**, *117*, 147–157.
51. Love, J.C.; Estroff, L.A.; Kriebel, J.K.; Nuzzo, R.G.; Whitesides, G.M. Self-Assembled Monolayers of Thiolates on Metals as a Form of Nanotechnology. *Chem. Rev.* **2005**, *105*, 1103–1169.
52. Zhao, C.L.B.; Dong, E.G. Electronic Structure of Short Carbon Nanotubes. *Mod. Phys. Lett.* **2003**, *17*, 375–382.
53. Malinsky, M.D.; Kelly, K.L.; Schatz, G.C.; Van Duyne, R.P. Chain Length Dependence and Sensing Capabilities of the Localized Surface Plasmon Resonance of Silver Nanoparticles Chemically Modified with Alkanethiol Self-Assembled Monolayers. *J. Am. Chem. Soc.* **2001**, *123*, 1471–1482.
54. Storhoff, J.J.; Lazarides, A.A.; Mucic, R.C.; Mirkin, C.A.; Letsinger, R.L.; Schatz, G.C. What Controls the Optical Properties of DNA-Linked Gold Nanoparticle Assemblies? *J. Am. Chem. Soc.* **2000**, *122*, 4640–4650.
55. Hillebrenner, H.; Buyukserin, F.; Kang, M.; Mota, M.O.; Stewart, J.D.; Martin, C.R. Functional Nanotube Templated Tubular Metal Shells. *J. Am. Chem. Soc.* **2006**, *128*, 4625–4627.